

R 0663

FEB 24 1986

APPENDIX V

NOWCASTING SEAICE MOVEMENT THROUGH THE BERING STRAIT

by

T.L. Kozo
W.J. Stringer
L.J. Torgerson

D111)

advance copy!
will be photographed
as is!

note: this is a refereed paper!
- essentially a
shortened form of the
M.W.R. copy

NOWCASTING SEAICE MOVEMENT THROUGH THE BERING STRAIT

Thomas L. Kozo

Occidental College, VANTUNA Research Group
Los Angeles, CA 90041

William J. Stringer

University of Alaska, Geophysical Institute
Fairbanks, AK 99701

Lenora J. Torgerson

University of Alaska, Geophysical Institute
Fairbanks, AK 99701

ABSTRACT

Geostrophic wind velocities were calculated using atmospheric pressure data from Bering Strait stations at Uelen (Siberia), Bukhta Provideniya (Siberia) and Nome (Alaska). These velocities were matched to Strait sea ice displacements derived from satellite imagery (1974-1984), resulting in an all-weather ice movement nowcasting model. Also, five ice displacement modes were identified.

The first mode is Chukchi to Bering Sea movement when northeasterly winds exceed 11.5 m/s. The second and third modes are Bering to Chukchi Sea movement. Mode two is driven by a preexisting north-flowing ocean current during weak opposing winds. Mode three is due to winds and currents acting in concert.

The first immobilization mode (maximum duration one week) is an apparent balance between northerly wind stress, water stress from the south, and internal ice stress. The second immobilization mode is due to large, double, solid ice arches jamming the Strait up to four weeks.

INTRODUCTION

Both northward and southward sea ice movement through the Bering Strait can be hazardous to oil development in the northern Bering Sea (Fig. 1, see for most place names). This wind- and current-dependent movement can be extensive from November to May and is connected to dynamic interactions with sea ice in the vicinities of St. Lawrence Island [1, 2] and Norton Sound [3].

There have been numerous papers since the seventies relating sea ice motion and oceanic transport in the Bering Strait to some type of meteorologic forcing. Sequential Landsat (National Aeronautics and Space Administration, NASA) and DAPP (U.S. Air Force) imagery was used to construct ice displacement vectors in the Strait [4]. A relationship between southward ice movement and northerly surface winds at Cape Wales was demonstrated. Analyses of National Oceanic and Atmospheric Administration (NOAA) surface synoptic weather charts explained episodes of alternating south and north sea ice motion [5] and several extensive southward

movements [6]. Similar extensive southward ice movements preceded by sea ice fracture, called "breakout," were modeled [7]. An atmospheric pressure difference from Cape Schmidt (Siberia) to Nome (Alaska) exceeding 20 mb was related to these events in the winters of 1975 and 1976. Atmospheric pressure differences (i. e., Provideniya to Nome) were also correlated with oceanic transport directions [8]. However, none of these differences were true pressure gradients, requiring a minimum of three simultaneous surface pressures. For example, the 20-mb pressure difference mentioned above amounts to a geostrophic wind of approximately 15 m/s from 40° only if the isobars are perpendicular to a line joining the reporting stations. It is shown in this paper that ice moves south through the Strait for a suite of geostrophic wind velocities often with Cape Schmidt to Nome pressure differences less than 20 mb.

New evidence for the feasibility of predicting ice movement from pressure-field wind calculation have been demonstrated [9]. National Weather Service (NWS) synoptic pressure data was combined with Fleet Numerical Oceanography Center (FNOC) techniques to predict theoretical surface winds for the Strait. A high correlation of oceanic transport to the meridional wind component in two different current-data collection years was found. Unfortunately, this last technique assumes a uniform surface wind field within 300 km of the Strait, which is highly improbable due to the preponderance of seaward propagating orographic effects in Arctic winters [10].

The main study objective is to create a nomogram for all-weather, short-term prediction or nowcasting [11] of sea ice movement through the Bering Strait from mesoscale network [12, 10] computed geostrophic wind velocities. The wind velocities are derived in a straightforward manner using an atmospheric pressure network encompassing the Bering Strait with three World Meteorological Organization (WMO) reporting stations: Uelen (U, Siberia), Provideniya (P, Siberia), and Nome (N, Alaska). The sea ice motion data were compiled from 11 years of daily visible and infrared NOAA 3-8 satellite image transparencies.

As a by-product of this study, three modes of ice movement and two modes of ice immobilization in the Strait have been identified and classified according to major driving forces.

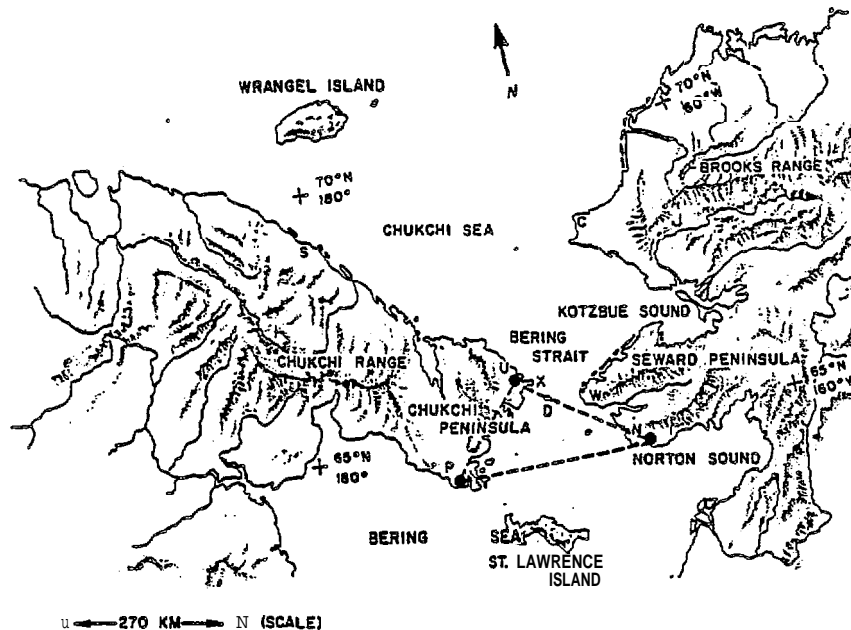


Fig. 1 The surface pressure station network P-U-N (dashed triangle) covering the Bering Strait region. P is Bukhta Provideniya, U is Uelen (both in Siberia) and N is Nome, Alaska. The Diomed Islands (D) are in the center of the Strait, Cape Schmidt (S) is below Wrangel Island, Cape Lisburne (C) is north of Kotzebue Sound, and Cape Wales (W) and Cape Dezhneva (λ) are on the tips of the Seward and Chukchi Peninsulas respectively. Mountain axes are shaded for emphasis.

STUDY AREA

The Bering Strait's oceanic cross section is roughly 85 km × 50 m and its annual average transport is ~0.6 Sv [9] to the north, attributed to higher sea level in the Bering Sea than in the Arctic Ocean [8, 13]. This relatively small annual northward transport would be five times greater if not for wind-induced flow reversals to the south occurring two to three times per month and lasting six to twelve days [14]. Daily mean transport can reach 3.1 Sv to the north [8] which implies currents up to 70 cm/s, given the above cross-sectional area. Current velocities of this magnitude are indications that oceanic flow driven north or south tends to be funneled (see Fig. 1) and accelerated on entering the Strait [15].

The same funneling applies to arctic winds in the Strait, which tend to flow around rather than over topography [10]. The Chukchi and Seward Peninsulas have small mountain ranges setting north to east and north to west respectively (Fig. 1). Their elevation are at least equal to 600 m, which is sufficient to redirect and accelerate air flow during winter conditions [16]. The Strait axis orientation was chosen to be 40°E from the north for comparison with earlier work [7].

DATA

Surface Atmospheric Pressure and Temperature

Barometric pressure data, reduced to sea level, and temperature data taken simultaneously from Uelen (66°10'N, 169°50'W), Bukhta Provideniya (64°26'N, 173°14'W), and Nome (64°30'N, 165°24'W) are used to

compute a geostrophic wind for the Bering Strait. The accuracies of these pressure and temperature data from Nome, a first-order weather station, are better than ±0.25 mb and ±1°C, respectively. The two Russian stations are part of a global network that transmits real-time data to the National Meteorological Center (NMC) and are assumed to be within these limits also.

Geostrophic Wind Data

These data were computed from the pressure and temperature data provided by the three above weather stations. The atmospheric flow was assumed to be in geostrophic balance, shown in Eq. (1):

$$f(k \times \nabla_G^P) + \frac{\nabla^2 P}{\rho} = 0 \quad (1)$$

The first term is the Coriolis force, and the second is the pressure gradient force. f is the Coriolis parameter ($1.321 \times 10^{-4} \text{ sec}^{-1}$ at 65°N), k is the vertical unit vector, ∇_G^P is the geostrophic velocity vector, $\nabla^2 P$ is the gradient of the atmospheric pressure, and ρ is the air density. Using station grid (Fig. 1), pressure can be represented as a function of latitude (Y) and longitude (x) on a plane surface:

$$\begin{aligned} P_N(x, y) &= ax_N + by_N + c \\ P_U(x, y) &= ax_U + by_U + c \\ P_P(x, y) &= ax_P + by_P + c \end{aligned} \quad (2)$$

The subscripts N, U, and P denote Nome, Uelen, and Provideniya, respectively. Cramer's rule can be applied to Eqs. (2) to solve for unknowns a, b, and c. Since $\partial P/\partial x = a$ and $\partial P/\partial y = b$, the pressure gradient (VP) can be computed. The geostrophic velocity (V_G) can now be calculated from Eq. (1) since f is known and p for dry air can be estimated from station temperatures.

Station errors of $\pm 1^\circ\text{C}$ (see above) in temperature can cause errors of 0.34% in the velocity magnitude since they affect ρ estimates. Station errors in pressure of ± 0.25 mb can cause maximum speed errors ± 1.4 m/s and direction errors greater than $\pm 15^\circ$ for wind speeds below 3 m/s. Therefore, at wind speeds ≤ 3 m/s, wind directions should not be considered significant.

Satellite Imagery

The ice-motion data came primarily from visible and infrared NOAA 3-8 VHRR (Very High Resolution Radiometer) satellite imagery. The infrared imagery was utilized mainly during December, January, and February when daylight was minimal. To minimize errors due to the earth's curvature, the scale was taken from the closest land mass. The net 24-h ice motion was measured directly by tracking identifiable floes or indirectly by measuring the change in ice edge location south or north of the Diomed Islands. A minimum of two days' imagery is necessary to document a displacement with an error estimated at ± 5 km.

During the ice-covered months (November through May) from 1974 to 1984, nearly 40% of the total observation days were obscured by undercast. However, the technique outlined below based on the remaining 60% of the data, if representative, will be an all-weather, under cast-independent predictive tool.

RESULTS WITH DISCUSSION

Constructing the Sea Ice Movement Prediction Nomogram

Net daily sea ice displacements derived from satellite imagery have been examined and compared to simultaneous mesoscale atmospheric pressure network (MAPN) computed V_G 's to produce an empirical nowcast nomogram (Fig. 2). Table 1 lists some of the events used in the nomogram construction and classifies them according to mode (major driving force) and zone (net movement and direction). The Greek and Latin letters from Table 1 are positioned in Fig. 2 to represent a MAPN-computed V_G (direction [from] and speed as independent variables). The small center circle represents V_G 's with speeds less than 3 m/s. Due to measurement errors and the minimal effects on ice motion at these low wind speeds, V_G 's within this circle should be considered as approximately zero winds. V_{θ} (see Table 1, definition B for sign) represents the V_G component parallel to the assumed Strait axis, 40° from north. This axis is indicated by ice movement direction arrows that meet in

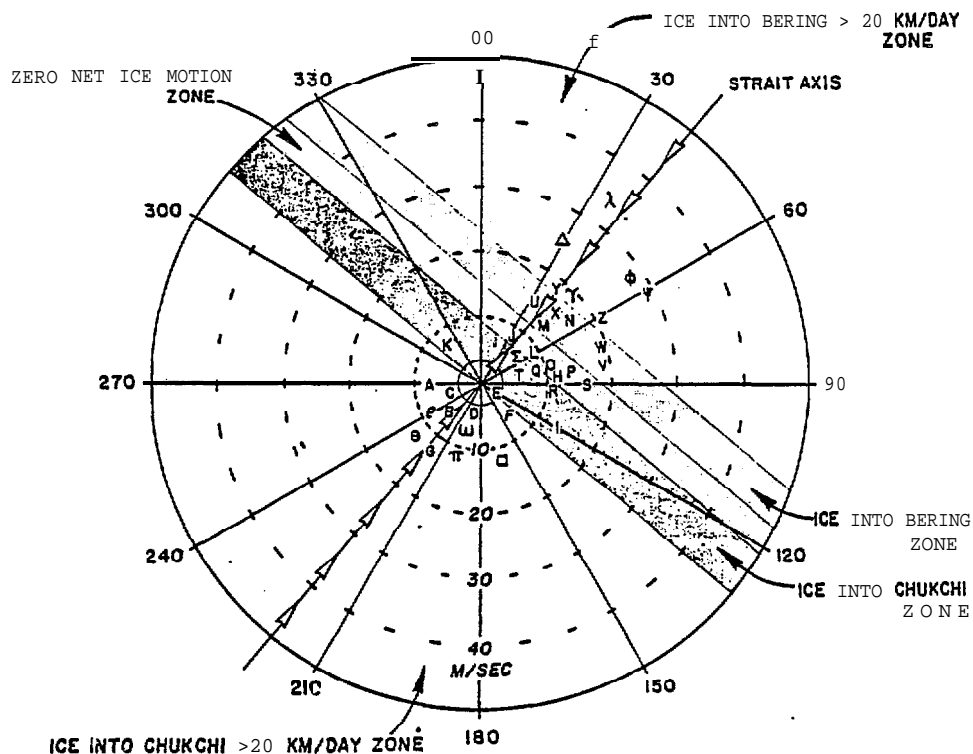


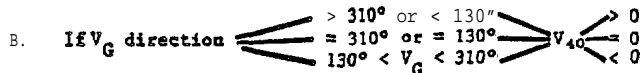
Fig. 2. The Bering Strait sea ice movement prediction nomogram with Greek and Latin letters representing sample MAPN-computed V_G 's used in its construction (see Table 1). The Strait axis is 40° from the north and has ice movement arrows meeting in the Zero Net Ice motion Zone. The center solid-line circle is the ≤ 3 m/s wind-speed zone and it represents direction uncertainties $> 15^\circ$.

TABLE 1. Selected net sea ice movement (I) events for the Bering Strait plotted in Fig. 2.

- Mode 1.** Into Bering Sea (wind-forced), winds opposed to normal ocean current direction.
- a. $I > 20$ Ion/day Zone ($V_{40} > 16.5$ m/s)
- Events: Y(14,15 Apr 82), Z(14,15 Mar 82)
 γ (17 Feb 81), A(17 Jan 83), Δ (11 Feb 84)
 ϕ (6,7 Mar 78), 41(27 Dec 76)
- b. $I < 20$ Ion/day Zone, (11.5 m/s $< V_{40} \leq 16.5$ m/s)
- Events: u(18 Feb 84), X(19 Feb 83), N(11 May 81)
V(22 Feb 76), W(27 Feb 79), M(2 May 77)
- Mode 2.** Into Chukchi Sea (ocean current forced, weak winds oppose current direction).
- a. $I < 20$ km/day Zone, (0 m/s $< V_{40} \leq 7.5$ m/s)
- Events: K(9 Apr 82), R(7 Dec 76), T(3 May 84)
Q(25 Feb 79), 1(23 Jan 82), Σ (21 Mar 75)
- Mode 3.** Into Chukchi Sea (major forces are ocean current and wind in the same direction)
- a. $I > 20$ km/day Zone, ($V_{40} < 0$ m/s), see Definition B below for direction.
- Events: G(8 Apr 82), Θ (6 Feb 82), Π (4 Feb 82),
P(22 Mar 78), \square (31 Jan 81), ω (24 Feb 82)
A(10, 11 Feb 79), B(16, 17 Feb 79), C(1,2 Feb 76)
11(27,28 Feb 76), E(5 May 84), F(2,3 Mar 82)
- Mode 4.** First immobilization mode, ocean current and wind in opposition (respective stresses apparently in balance)
- a. Zero Net Ice Movement Zone ($I = 0$)
(7.5 m/s $< V_{40} \leq 11.5$ m/s)
- Events: J(23 Mar 82), S(21 Feb 76), H(24 Jan 83)
L(21 Apr 81), O(11 Apr 78), P(2 Apr 78)

Definitions:

A. $V_{40} \equiv V_G$ speed component parallel to Strait axis $40^\circ E$ from north (Fig. 2).



the Zero Net Ice Motion Zone, one of five zones defined by wind-speed ranges along the V_{40} axis. These nomogram zones are used to characterize three motion modes and one immobilization mode in the Strait. A fifth mode, though not yet predictable, was a discovery of this procedure and will be discussed later.

Mode 1 contains two zones of wind-forced sea ice movement into the Bering Sea which initially must offset a northward-flowing ocean current [9, 13]. The threshold for southward movement is a V_{40} exceeding 11.5 m/s. The bounds on V_{40} for each zone are shown in Table 1 and Fig. 2. The >20 Ion/day Zone conditions would push an amount of ice into the Bering Sea sea approximately equal to double the area of St. Lawrence Island for five days. Examples of mode 1 occurred 11, 20, and 27 December 1976, during total ice cover when the Bering Strait ocean current at 10 m from the bottom switched from north to south [8]. The average MAPN-computed V_{40}

during these three cases was 29 m/s from 61° (ψ , Fig. 2). The 27 December 1976 event, with clear satellite imagery, showed net southward Strait ice movement of 23 km.

Mode 2 includes only one nomogram zone. Sea ice movement is northward into the Chukchi Sea, and this mode is ocean current dominated with minor opposing wind influence. The northward movement represented by the ICE INTO CHUKCHI ZONE with 0 m/s $\leq V_{40} \leq 7.5$ m/s, is due to a preexisting northward-flowing ocean current that overpowers the weak opposing wind. A V_G approximately 60% of V_{40} [7.5 m/s] is 4.5 m/s or the wind equivalent of a gentle breeze. Nevertheless, the net northward sea ice movement is reduced to less than 20 km/day. This current appears to be a combination of residual contributions [17] from the Bering Sea side and a permanent downward sea level slope [8] from the Bering toward the Chukchi of steric origin [13].

page number 

PLEASE CAREFULLY READ EXPLOSION AUTHORITY'S INSTRUCTIONS

Mode 3 includes the ICE INTO CHUKCHI >20 km/day ZONE with $V_{40} \leq 0$. The wind and water stress are in the same direction. All wind speeds in this mode produce northward ice motion adjacent to Norton Sound and Chukchi sea ice injections of double the SLI area in five days. However, higher wind-speed events (> 5 m/a) have sometimes produced less net movement than the low-wind-speed or current-dominated events. The nomogram breakdown of the net daily sea ice motion into 20-km slots despite satellite imagery displacement accuracy of ± 5 km is a result of this phenomenon. This indicates that opposing internal and boundary ice stresses may play an important role at higher wind speeds.

Mode 4 is one of zero net ice movement, usually lasting less than one week, with $7.5 \text{ m/s} < V_{40} < 11.5 \text{ m/a}$. The primary force balance in the Strait area is between the wind stress pushing ice south and the water stress pushing ice north. The relative magnitudes of the opposing surface wind stress (τ_w) and water stress (τ_w) are quite comparable and add credibility to the nomogram design (see Appendix A).

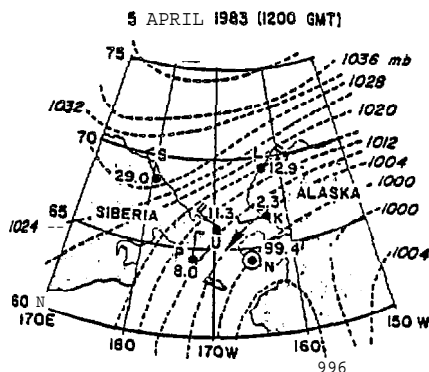


Fig. 3. Orographic effects on surface wind velocities despite a well defined isobaric pattern (dashed lines). The numbers adjacent to sites are surface pressures in mb minus 1000, unless the number is greater than 60, then pressures are in mb minus 900. Surface wind speeds are $\sqrt{2}$ m/a for each perpendicular flag, $\sqrt{2.5}$ m/s for slant flags, and $\sqrt{0}$ for a circle (i. e., N). The stations shown are Provideniya [P], Uelen [U], Home [N], Kotzebue [K], Point Lay [L], and Cape Schmidt [S]. The MAPN-computed V_G is shown by the arrow.

Using the Nomogram

Simultaneous surface-pressure and temperature data from Uelen, Provideniya, and Nome for 00 and 1200 GMT should be available to the user less than three hours after recording at the respective stations. These data (P_N, P_U, P_P) can be combined with Eq. (2) to solve for VP . Air density (ρ) is approximated using a three-station average temperature and the equation of state for dry air, $p = P/RT$. P is the standard sea level atmospheric pressure (1013.3 mb), R is the gas constant, and T is the absolute temperature. The solution for VP , p and V_G can be obtained from Eq. (1). The V_G for 00 and 1200 GMT are combined to obtain an average velocity (V_G). Once V_G is known, the two necessary independent variables speed (V_G radius vector) and direction (vectorial

angle), can be plotted on polar-coordinate graph paper with the nomogram's five wind speed zones and V_{40} axis superimposed. For example, using data from Fig. 3, $P_N = 999.4 \text{ mb}$, $P_U = 1008.0 \text{ mb}$, $P_P = 1011.3 \text{ mb}$, and an average temperature of -5°C (not shown), $V_G = 23 \text{ m/s}$ from S6. S (see arrow). Plotting this value (X) on Fig. 4 (bottom) and drawing a perpendicular from the V_{40} axis to X predicts net ice movement >20 km/day to the south. The net ice movement obtained from satellite imagery was 45 km south.

Testing the Nomogram Technique

MAPN advantages over other techniques. Figure 5 demonstrates the MAPN advantage over both pattern recognition and NMC synoptic analysis. A type of "relaxed" atmospheric pressure field has existed for four days, which from pattern-recognition analyses [18] denotes probable northward ice movement. However, the MAPN-calculated geostrophic wind velocity indicates that the "brakes" are being applied to northward sea ice movement. The 1200 GMT, 25 March 1978 V_G was 11.0 m/e from 75° , and the average V_G for the next 12-h period was 12.4 m/s from 68.4° . The net ice movement switched from north to 6 km south by 26 March.

The effects of orography are striking, even with a well-defined surface pressure pattern as demonstrated on 5 April 1983 (Fig. 3). The large variations in direction and speed of surface winds at P, U, and N are evidence that previous attempts [7, 15] to correlate 10CS1 winds with ice movement or ocean current direction in their vicinity met with limited success.

These above examples show also the dangers of using pure synoptic analyses to derive the surface wind field. In their most recent work [9], an error is made by assuming the derived surface wind field to be uniform within 300 km of the Strait.

NOAA satellite imagery. A time period having 23 consecutive undercast-free days (6-24 April 1982) was chosen to test the accuracy of the MAPN and nomogram predictions. The numbers 6-2S are April dates and represent the V_G positions combining the 00 and 1200 GMT V_G 's on those days (Fig. 4, bottom). If the wind direction changed by more than 90° in 12 h, and/or the change reversed the direction of ice motion, no prediction would be made. If any of the three network stations failed to report at either the 00 or 1200 GMT time periods, then the closest available simultaneous time periods were used for the V_G . Figure 4 (top) shows the net sea ice movement in km derived from satellite imagery for the corresponding days. Allowing for the error bounds on the imagery (± 5 km) and the V_G ($\pm 1.4 \text{ m/a}$), the nomogram technique failed in only 2 cases out of 23 and was 91% correct.

The first case was 12 April 1982 where a V_G of 14 m/s from 22° produced 36 km of actual southward ice movement instead of the <20 km south predicted. The second case on 25 April 1982 had 16 km net northward sea ice movement shown on the satellite imagery. The MAPN V_G of 10.2 m/a from 31.4° predicted zero net motion.

Buoy drift data. The nomogram technique was applied in hindcast fashion to recent buoy drift data in the Strait area [19]. Though this data is of a different type than the satellite imagery, the MAPN prediction was correct for 33 of 39 days or $\sim 85\%$. The present MAPN does not include corrections for conditions of rapidly changing atmospheric pressure (isallobaric effect) or cases where the isobaric radius of curvature is less than 300 km [20]. These refinements can be built into the wind-velocity calculation and on application to the nomogram appear to increase the accuracy $\sim 5\%$.

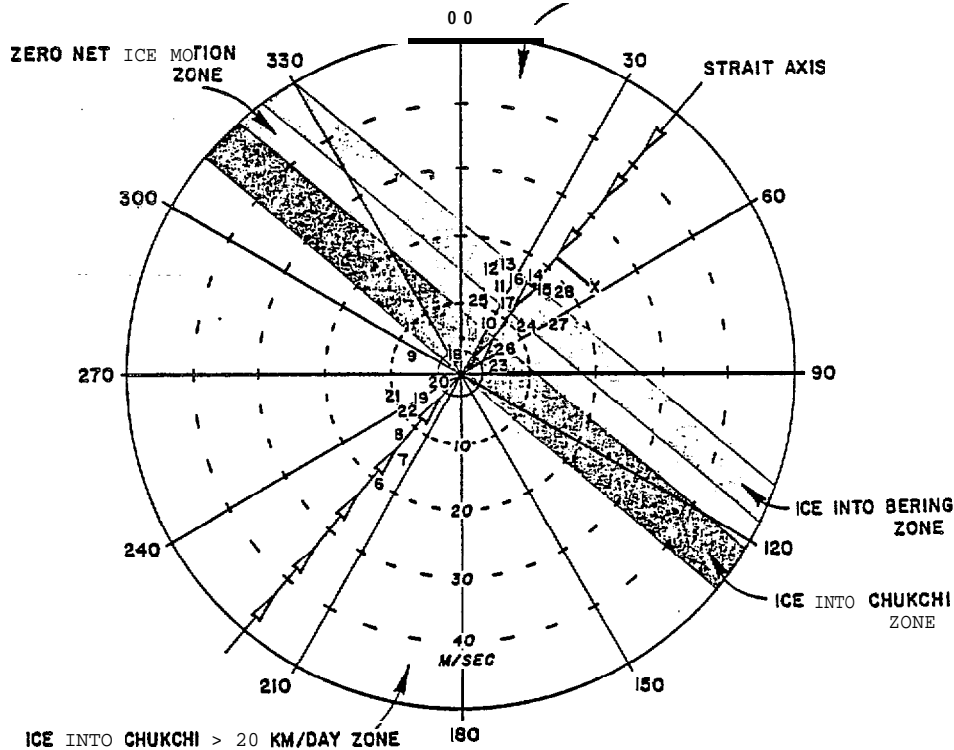
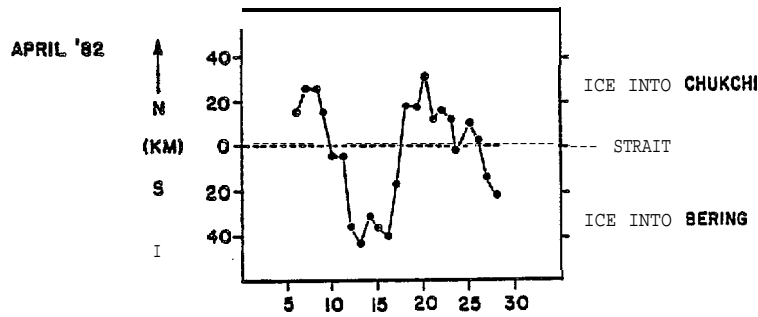


Fig. 4. Satellite imagery derived ice displacement (top) compared to MAPN \vec{V}_G 's for 6-28 April 1982 plotted with corresponding day numbers on the sea ice movement prediction nomogram (bottom). The number positions represent wind velocity vectors whose V_{40} components define the daily predicted ice movement zone. X is a sample V_G calculated from surface pressure data in Fig. 3. Drawing a perpendicular line from X to the Strait axis results in a $V_{40} = 22$ m/s. This is the Ice Into Bering >20 km/day Zone.

Solid, Double Sea Ice Arches (Mode 5)

The double sea ice arch represents the longer duration second mode of ice immobilization. Only five cases (a possible sixth was noted on Landsat Data for 5 April 1976) have been found in 11 years of sea ice satellite data. A photograph made from a satellite image (Fig. 6) taken 5 May 1980 shows the characteristic solid, double ice arch using the tip of the Chukchi Peninsula (Cape Dezhneva), the Diomed Islands, and the Seward Peninsula tip (Cape Wales) as anchor points. Since the image chosen was taken 21 days after the

arches formed, it appears that it was not cold enough for new ice formation and the presence of arches prevented resupply by old ice advection from the north. These arches are not the arched fractures seen in sea ice during failure modes [2, 7] but evidently represent strong impedimenta to southward sea ice movement (see Appendix B for details). As evidence of the lack of fractures in the ice canopy during the solid-arch phase, the above (14 April to 10 May 1980) period represented a halt in whale (Bowhead) migration through the Strait (Huford, 1984, National Weather Service, Anchorage, pers. comm.).

The double arches were discovered indirectly through failure of the nomogram prediction system. In all double-arch cases, the nomogram with V_G from the MAPN predicted greater than 20 km/day of net ice movement into the Bering for at least 50% of the arch period. There were several V_G 's as high as 26 m/s with no ice movement. In addition, the greater than 20 mb pressure difference ice breakout criterion [7] from Cape Schmidt to Nome was exceeded at some time during all the double-arch periods.

SUMMARY AND CONCLUSIONS

The combination of MAPN-calculated V_G 's with the nomogram provides an all-weather Bering Strait sea ice movement nowcasting capability with an accuracy of approximately 85%. The MAPN improvement over NMC surface pressure analyses and pattern-recognition techniques has been demonstrated. This study, though meteorologically oriented, has also shed light on oceanographic phenomena.

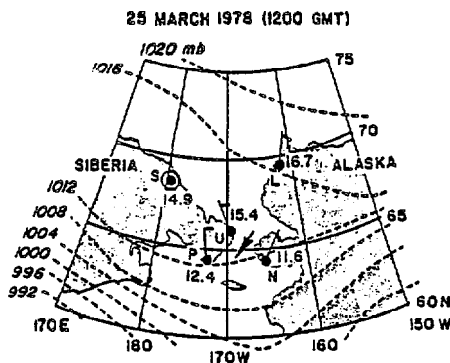


Fig. 5. An example of the advantages of the MAPN analysis over both pattern recognition and NMC surface isobaric analysis. The station, surface pressure, flag, and V_G designations are as in Fig. 5.

Sea Ice Movement Modes

Three modes of ice movement were found. The first is a southward atmospherically forced movement into the Bering Sea requiring a $V_{40} > 11.5$ m/s to offset a pre-existing north-flowing ocean current. The second mode is current-forced movement into the Chukchi Sea offsetting weak opposing synoptic winds ($V_{40} < 7.5$ m/s). The third mode is usually large northward ice movement (>20 km/day) under the influence of southwest winds and a north-flowing ocean current.

Sea Ice Immobilization Modes

There were two ice immobilization modes found in the Strait. The first is an apparent balance between wind stress from the north and a current-induced water stress from the south. This mode is short term, usually lasting less than one week. The second mode was found only 5 times in 11 years. Double, solid sea ice arches, made possible by the Diomed Islands anchoring their middle column, were the apparent cause. A theoretical estimate of the double-arch strength showed the ability to withstand the V_G 's generated during the arch periods. This longer-period immobilization mode (up to four weeks) can hinder spring whale migration into the Chukchi and sid in opening up the region below the Strait as well as Norton Sound.

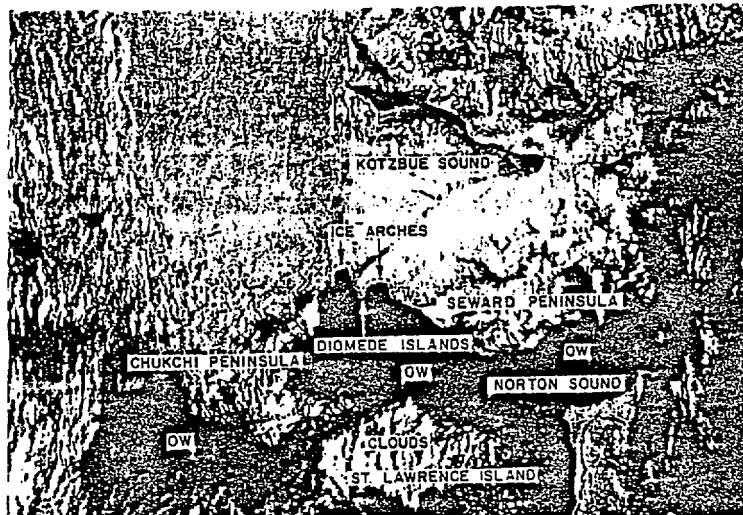


Fig. 6. A photograph made from a satellite image taken May 5, 1980, showing the characteristic solid, double ice arch in the Bering Strait. There is a large expanse of open water (OW) south of the Strait, south of the Chukchi Peninsula and in Norton Sound.

APPENDIX A

Comparison of Wind (τ_a) and Water (τ_w) Stress

$$\tau_a = \rho_a C_a (U_a \cdot r_a)^2 \quad (A1)$$

$$\tau_w = \rho_w C_w U_w^2 \quad (A2)$$

where (using values typical of the Strait conditions)

ρ_a = density of dry air at $-20^\circ\text{C} \sim 1.3 \text{ kg/m}^3$

C_a = 10 m drag coefficient [21] for air/water $\sim 3 \times 10^{-3}$

U_a = average wind speed in the Zero Net Ice Motion Zone $\sim 10 \text{ m/s}$

r_a = ratio of surface wind speed (10 m) to the calculated geostrophic wind ~ 0.6 for arctic conditions [22]

ρ_w = density of water at $0^\circ\text{C} \sim 1 \times 10^3 \text{ kg/m}^3$

C_w = 2 m drag coefficient [23] for ice/water $\sim 16 \times 10^{-3}$

U_w = current speed due only to tidal residuals in the Bering Strait area $\sim 0.1 \text{ m/s}$ [17]. This assumes that the usual sea surface slope downward to the north [9, 13] driving the mean flow is all but eliminated by a V_{40} of 10 m/s.

After inserting these values in Eq. (A1) and Eq. (A2):

$$\tau_a = 0.15 \text{ N/m}^2; \tau_w = 0.16 \text{ N/m}^2$$

APPENDIX B

Estimating Arch Strengths

Work by Sodhi [2] will be used to show the reason for double arch existence despite the strong MAPN winds. Figure 7 is an enlargement of the Strait area from Fig. 6. The dashed curves differentiate the sea ice arches from the coastal boundaries and the dark areas are open water. The single-arch strength can be

estimated by comparing the arches in Fig. 7 to the inset drawing. The span width ($2A$) of the arch from the Diomede Islands to the Seward Peninsula is 43 km and from the Chukchi Peninsula to the Diomedes is 37 km. The width of the Diomede Island blockage zone is 7 km [1]. The eastern arch (Diomede Islands-Seward Peninsula) has a $\theta \sim 80^\circ$ while the western arch (Diomede Islands-Chukchi Peninsula) is more irregular with an average θ of $\sim 80^\circ$ also. From Eq. (B1)

$$\theta = \pi/4 + \phi/2 \quad (B1)$$

where ϕ = angle of internal friction

θ = see Fig. 7

ϕ is estimated as 70° for both arches. Next Eq. (B2) is used to solve for τ as defined by Eq. (B3).

$$\lambda = \frac{c}{\tau} (1 + \sin \phi) \quad (B2)$$

$$\tau = \rho c V^2 \quad (B3)$$

Here [2]:

λ = half span width (m)

c = cohesive strength (N/m)

τ = net stress per unit area (N/m^2) (wind and water stress combined)

ρ = medium density (kg/m^3)

C = drag coefficient (unitless)

V = wind velocity (m/s)

"Cohesive strength (c) for Amundsen Channel (Beaufort Sea, June) sea ice in a solid arch was estimated from Eq. (B2) and Eq. (B3) at failure to be 1993 N/m [2]. The net stress (τ) applied to this arch (zero water stress assumed) was calculated using a typical 10-m air-ice drag coefficient of 1×10^{-3} for C and local winds for V . Recent Bering Sea work [9] shows C

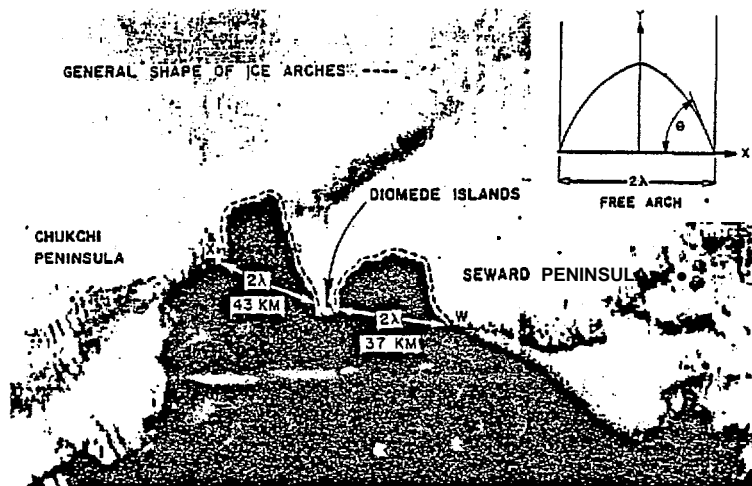


Fig. 7. An enlargement of the Strait area taken from the Fig. 6 photograph. The dashed curves show the actual "sea ice arches" to avoid confusion with land boundaries. The large dark area is open water. The inset (top) is a sketch of an idealized free arch showing the span width ($2A$) and the angle (θ) between the horizontal and tangent to the free surface.

to be three times the Sodhi [2] estimate resulting in $c = 5979 \text{ N/m}$ as the cohesive strength of sea ice at failure. Given this c , taking $\phi = 70^\circ$, and $\lambda \sim 20 \times 10^3 \text{ m}$ (double arches) and substituting into Eq. (B2), τ (net) = 0.58 N/m^2 .

Remembering that water stress generally opposes wind northerly stress, τ_w is estimated to be -0.16 N/m^2 from Eq. (A2). The air stress τ_a is calculated from Eq. (B4):

$$\tau = \tau_a + \tau_w \quad (B4)$$

Therefore $\tau_a = (0.58) - (-0.16) = 0.74 \text{ N/m}^2$.

Hence from Eq. (A1)

$$U_a = 23 \text{ m/s} = V_{40} \text{ on the nomogram axis.}$$

V_{40} converts [22] to a surface wind speed of 13.8 m/s. This speed occurs less than 10% of the time [24] at Tin City (near Cape Wales, Fig. 1). The estimated V_{40} value of 23 m/s is close to the maximum V_{40} of 26 m/s calculated for three of the arch cases. The cohesive-strength estimate used here could have been slightly larger since no evidence of arch breakup during these winds existed. The observed manner of double arch destruction is a relaxation of the northerly wind and a switch to pure water stress or combined wind and water stress from the south.

ACKNOWLEDGMENTS

This study was funded by the Minerals Management Service, U.S. Department of the Interior, through inter-agency agreement with the National Oceanic and Atmospheric Administration, U.S. Department of Commerce, as part of the Outer Continental Shelf Environmental Assessment Program.

REFERENCES

- Shapiro, L. H., and Burns, J. J., "Major late-winter features of ice in Northern Bering and Chukchi Seas as determined from satellite imagery", Geophys. Rept., No. UAG-R-236, Sea Grant Rpt. No. 758, Univ. of Alaska, Fairbanks, 1975, 14 pp.
- Sodhi, D. S., "Ice arching and the drift of pack ice through restricted channels", Cold Regions Research and Engineering Laboratory CRREL Rpt. 77-18, Hanover, NH, 1977, 11 pp.
- Stringer, W. J., and Hufford, G. L., "Interaction of Bering Sea and Norton Sound pack ice", Arctic and Alpine Res., 14, 1982, pp. 149-156.
- Shapiro, L. H., and Burns, J. J., "Satellite observations of sea ice movement in the Bering Strait region", in Climate of the Arctic, Univ. of Alaska, Fairbanks, 1975, pp. 379-386.
- Ray, V. M., and Dupre, W. R., "The ice-dominated region of Norton Sound and adjacent areas of the Bering Sea", Chapter 16 in The Eastern Bering Sea Shelf: Oceanography and Resources (ed. by D. W. Hood and J. A. Calder) Univ. of Washington Press, Seattle, 1981, pp. 263-278.
- Kovacs, A., Sodhi, D. S., and Cox, G. F. N., "Bering Strait sea ice and the Fairway Rock icefoot", Cold Regions Research and Engineering Laboratory, CRREL Rpt. 82-31, Hanover, NH, 1982, 40 pp.
- Reimer, R. W., Pritchard, R. S., and Coops, M. D., "Beaufort and Chukchi Sea ice motion: Part 2. Onset of large scale Chukchi Sea ice breakout", Flow Res. Rpt. No. 133, Kent, WA, 1979, 92 pp.
- Coachman, L. K., and Aagaard, K., "Reevaluation of water transports in the vicinity of Bering Strait", Chapter 7, in The Eastern Bering Sea Shelf: Oceanography and Resources, (ed. by D. W. Hood and J. A. Calder), Univ. of Washington Press, Seattle, 1981, pp. 95-110.
- Aagaard, K., Roach, A. T., and Schumacher, J. D., "On the wind-driven variability of the flow through the Bering Strait", J. Geophys. Res., 90, 1985, pp. 7213-7221.
- Kozo, T. L., "Mesoscale wind phenomena along the Alaska Beaufort Sea Coast", in The Alaska Beaufort Sea: Ecosystems and Environment (ed. by P. W. Barnes, D. M. Schell and E. Reimnitz), Academic Press, New York, 1984, pp. 23-45.
- Browning, K. A., Preface in Nowcasting, (ed. by K. A. Browning), Academic Press, New York, 1982, pp. IX-XI.
- Kozo, T. L., "Mountain barrier baroclinicity effects on surface winds along the Alaskan Arctic Coast", Geophys. Res. Ltrs., 7, 1980, pp. 377-380.
- Stigebrandt, A., "The North Pacific: A global-scale estuary", J. Phys. Oceanogr., 14, 1984, pp. 464-470.
- Kovacs, A., and Sodhi, D. S., "Sea ice piling at Fairway Rock, Bering Strait, Alaska: observations and theoretical analyses", Proc. Sixth Int. Conf. on Port and Ocean Eng. under Arctic Cond. POAC-81, Quebec, Canada, 2, 1981, pp. 985-999.
- Coachman, L. K., Aagaard, K., and Tripp, R. B., Bering Strait: the regional physical oceanography, Univ. of Washington Press, Seattle and London, 1978, 172 pp.
- Dickey, W. W., "A study of a topographic effect on wind in the arctic", J. Meteor., 18, 1961, pp. 790-803.
- Liu, S. K., and Leenderate, J. J., "Modeling the Alaskan coastal waters", Raad Rpt. R-3236-NOAA 85, 1985, 206 pp. (Available from the Raad Corporation, Santa Monica, CA, and National Ocean Service, Anchorage, Alaska.)
- Hufford, G., and Scheidt, R., "Interaction of Norton Sound Ice and Weather", Abstr. in 1984 Arctic Science Conference, (35th Alaskan Conference), Oct. 2-5, 1984, Anchorage, Alaska, sponsored by Amer. Assn. for Adv. of Sci.-Arctic Div., Amer. Met. Soc., and Arctic Inst. of North America, Anchorage, 1984, 109 pp.
- Reynolds, M., and Pease, C. H., "Drift characteristics of the northeastern Bering sea ice during 1982", NOAA Tech. Memo. ERL-PHIL-55, Sea tt Le, WA, 1984, 135 pp. (Available as PB 84-213982 from the Natl. Tech Inf. Serv., Springfield, VA.)
- Kozo, T. L., "An observational study of sea breezes along the Alaska Beaufort Sea Coast: Part 1.", J. App. Meteor., 12, 1982, pp. 891-905.
- Walter, B. A., Overland, J. E., and Gilmer, R. O., "Air-ice drag coefficients for first-year sea ice derived from aircraft measurements", J. Geophys. Res., 89, 1984, pp. 6525-6531.
- Albright, T. L., "Geostrophic wind calculation for AIDJEX", in Sea Ice Processes and Models, edited by Robert S. Pritchard, Univ. of Washington Press, Seattle, 1986, pp. 402-409.
- Pease, C. H., and Overland, J. E., "An atmospherically driven sea-ice drift model for the Bering Sea", Arctic Glaciol., 5, 1984, pp. 111-113.
- Brewer, W. A., Diaz, H. F., Prechtel, A. S., Searby, H. W., and Wise, J. L., Climatic Atlas of the Outer Continental Shelf Waters and Coastal Regions of Alaska, National Climatic Center (NCC), Asheville, NC, 1977, 409 pp.



**Executive Committee
1985-1986**

Chairman

Dr Jin S. Chung
Colorado School of Mines
Dept. of Engineering
1500 Hill Street
Golden, CO 80401
303-441-1900
fx. 0190 CSM GLDN

First Vice Chairman

Dr Virginia J. Lunardini
U.S. Army Cold Regions
Research & Engng Lab.
72 Lyres Road
Hanover, NM 03755
502.646-4325
TWX 710*266-1626

Treasurer

Dr Subrata K Chakrabarti
cm Industries, Inc
1501 North Division Street
Plainfield, IL 60544.8929
635-436.2912
TLX. 253166
62664 Intl Telex.

Secretary

Joseph W Galate
Enertech Engineering & Research Co
(Sic-1000)
5847 San Felipe Road
Houston, TX 77096
713-789-0055
TLX. 203256 ACTHUR

Member

Dr David L Garrett
Mobil Oil Corp
P.O. 601900
Dallas, TX 75221
214-671-1111

Member

Dr O.A. Ayirinde
Exxon Production Research Co
P.O. Box 2189
Houston, TX 77001
713-965-4911
TLX 910-881-5579
USEPR TX HOU

ASME Group Director

Wen T. Chow
345 E. 47th Street
New York, NY 10017
2s2-70s.70s5

ASME Technical Administrator

Wayne A Carmil
345 E 47th Street
New York, NY 10057
212-705-7284

Membership Services

Os O.A. (Fam) Ayirinde
Exxon Production Research Co
P.O. Box 2189
Houston, TX 77001
713-965-4911
fx. 910-881-5579
USEPR TX HOU

International Committee

Dr Jin S Chung
Colorado School of Mines
Dept 01 Engineering
1500 Hill Street
Golden, CO 80401
303-441-1900
TLX 5 0190 CSM GLDN

Calgary Chapter

Dr Edward W. Gregory
Petro-Canada Ltd.
P.O. Box 2544
Calgary A6 T2P 3E3 CANADA
405-255-5214
fx. 025257s3

Houston Chapter

Joseph W Galate
Enertech Engineering & Research Co.
(Sic-1000)
5647 San Felipe Road
Houston, TX 77056
713-789-0055
TLX. 203218 ACTH UR

November 11, 1985

Dear Corresponding OMAE Authors:

Congratulations ! It is our pleasure to inform you that your paper has been accepted for presentation at and for inclusion in the Proceedings of the Fifth (1986) International Symposium & Exhibit on Offshore Mechanics and Arctic Engineering (OMAE), Tokyo. Two Panel Sessions and 51 technical Paper Sessions with reviewed papers have been scheduled.

Enclosed are:

- (1) 1986 OMAE Advance Program with Call for Papers for 1987 OMAE Houston
- (2) "Presenting Your Paper (143-4A), " and Session Check list
- (3) Author /Panelist Informations Form (complete and return this Form by March 17, 1986 to Tokyo). Don't forget OMAE-number. Standard equipment (35-mm slide projector and overhead projector for transparency) are available in each room.

At your arrival at Keio Plaza Hotel, pick up your badge and a set of Proceedings (4th Floor), and contact Session Chairman or Co-Chairman in the Session Assignment Table (to be provided later in January). You may give 6-lines introduction (education, Specialties , employers and title) each of yourself and the coauthors to the Session Chairman at the Author Brief ings (4th Floor) for the introduction of your presentation.

If the presenting author encounters any last minute problem of not being able to present your paper, please inform us promptly. We suggest you would advance-register or preregister before the end of 1985. Find the Program "special discount airfare coupon" from North America and Europe. If you wish to visit OMAE Workshop, China and some sight-seeing following the OMAE Tokyo, see the backside of this letter for more information.

In order to accommodate the overflow of accepted papers, we scheduled nearly -twice more sessions (over the hotel capacity) and Proceedings pages than the original plan. This means that sessions are a little crowded, and consequently the registration fee had to be slightly increased.

The 1986 OMAE Technical Program Committee would like to welcome you to the exciting Fifth Symposium and will be looking forward to meeting you.

SEASONS GREETINGS !

Jin S. Chung, Chairman
The 1986 OMAE Tokyo Symposium

Encl.

(more on backside)